Available online at www.sciencedirect.com
ScienceDirect
Trans. Nonferrous Met. Soc. China 28(2018) 2470−2477
Transactions of Nonferrous Metals Society of China
www.tnmsc.cn

Microstructure and remarkably improved hydrogen storage properties of Mg_2Ni alloys doped with metal elements of Al, Mn and Ti

Hai-chang ZHONG[1,2], Jing-bo XU[2], Chun-hai JIANG[1,2], Xiang-jun LU[1,2]

1. Fujian Provincial Key Laboratory of Functional Materials and Applications, Xiamen University of Technology, Xiamen 361024, China;
2. School of Materials Science and Engineering, Xiamen University of Technology, Xiamen 361024, China

Received 26 December 2017; accepted 16 April 2018

Abstract: $Mg_2Ni_{0.7}M_{0.3}$ (M=Al, Mn and Ti) alloys were prepared by solid phase sintering process. The phases and microstructure of the alloys were systematically characterized by XRD, SEM and STEM. It was found that Mg_3MNi_2 intermetallic compounds formed in $Mg_2Ni_{0.7}M_{0.3}$ alloys and coexisted with Mg and Mg_2Ni, and that radius of M atoms closer to that of Mg atom was more beneficial to the formation of Mg_3MNi_2. The hydrogen storage properties and corrosion resistance of $Mg_2Ni_{0.7}M_{0.3}$ alloys were investigated through Sievert and Tafel methods. $Mg_2Ni_{0.7}M_{0.3}$ alloys exhibited remarkably improved hydrogen absorption and desorption properties. Significantly reduced apparent dehydriding activation energy values of −46.12, −59.16 and −73.15 kJ/mol were achieved for $Mg_2Ni_{0.7}Al_{0.3}$, $Mg_2Ni_{0.7}Mn_{0.3}$ and $Mg_2Ni_{0.7}Ti_{0.3}$ alloys, respectively. The corrosion potential of $Mg_2Ni_{0.7}M_{0.3}$ alloys shifted to the positive position compared with Mg_2Ni alloy, e.g. there was a corrosion potential difference of 0.110 V between $Mg_2Ni_{0.7}Al_{0.3}$ alloy (−0.529 V) and Mg_2Ni (−0.639 V), showing improved anti-corrosion properties by the addition of Al, Mn and Ti.
Key words: Mg_2Ni; Mg_3MNi_2; hydriding kinetics; dehydriding activation energy; anti-corrosion properties

1 Introduction

Mg-based alloys were regarded as a candidate of the most promising hydrogen storage materials [1]. Typically, Mg_2Ni had been intensively investigated as a gaseous hydrogen storage alloy and negative electrode material of nickel−metal hydride (Ni–MH) battery [2]. As a hydrogen storage material, its sluggish kinetics should be improved, and the operation temperature needed to be lowered. Therefore, tremendous efforts had been devoted to investigate and improve the hydrogen storage properties of Mg_2Ni. Ball milling and rapid quenching were widely used to fabricate amorphous/nanocrystalline Mg_2Ni for enhancing the hydrogen absorption and desorption [3]. Alternatively, novel synthetic techniques, such as hydriding combustion synthesis (HCS) and hydrogen plasma metal reaction technique, were developed to synthesize Mg_2Ni for further improving the hydrogen absorption/desorption kinetics [4,5]. Furthermore, it was observed that the absorption/desorption kinetics of Mg_2Ni could be significantly improved by doping with metals, such as V, Cr, Fe, Co and Cu [6]. For example, the hydrogen desorption activation energy of Mg_2Ni was lowered to 50.50 kJ/mol by doping with La and Cu through rapid quenching [7]. Although encouraging progresses had been achieved by alloying, element substitution, nanocrystallization and so on [8−11], it still could not meet the requirements for on-board utilization.

On the other hand, Mg_2Ni base alloys were regarded as one of the most promising negative electrode materials for Ni−MH battery due to the high theoretical capacity and low cost. However, the actual capacity of crystalline Mg_2Ni alloy electrode was not so high as expected, and the cyclic property was very poor [12]. The amorphous Mg_2Ni alloy obtained via ball milling showed superior discharge capacity [2]. While the amorphous Mg_2Ni suffered from serious corrosion and most capacity was lost within several charge−discharge cycles [13,14]. So, enhancing anti-corrosion and improving cyclic stability were also imperative for the Mg_2Ni-based alloy electrodes.

Doping metal elements was a traditional and

Foundation item: Project (2016J01266) supported by the Natural Science Foundation of Fujian Province, China; Project (JZ160474) supported by the Science and Technology Project of Education Department of Fujian Province, China
Corresponding author: Hai-chang ZHONG; Tel: +86-592-6291337; Fax: +86-592-6291328; E-mail: chunghc@163.com
DOI: 10.1016/S1003-6326(18)64893-9

effective way to improve the hydrogen storage properties of Mg-based alloys [15,16]. Interestingly, it has been recently reported that introducing some metals into Mg_2Ni would form kinds of FCC-structure new ternary intermetallic compounds, such as Mg_3MnNi_2, Mg_3AlNi_2, Mg_3TiNi_2 and Mg_3GeNi_2. Mg_3AlNi_2, Mg_3TiNi_2 and Mg_3MnNi_2 alloys were found readily absorbing/desorbing hydrogen, and a new metal hydride $Mg_3MnNi_2H_3$ was observed [17,18]. Moreover, those ternary intermetallic compounds exhibited better electrochemical properties compared with the binary Mg_2Ni alloy.

As well known, there were "synergetic or pump effects" during hydriding and dehydriding processes when Mg-based alloys composited with some readily hydrogen absorption/desorption alloys, such as AB_5 alloy [19]. However, it was still unknown whether and how Mg_3MNi_2 would affect the hydrogen storage properties of Mg-based alloys. Herein, a series of alloys with nominal compositions of $Mg_2Ni_{0.7}M_{0.3}$ (M = Al, Mn and Ti) were prepared. The phase component, phase structure and microstructure of the alloys were characterized by powder X-ray diffractometry (XRD), scanning electron microscopy (SEM) and scanning transmission electron microscopy (STEM). The hydrogen storage properties were systematically investigated by Sievert method, and the corrosion resistance performance was evaluated through Tafel measurement. As a consequence, $Mg_2Ni_{0.7}Al_{0.3}$, $Mg_2Ni_{0.7}Mn_{0.3}$ and $Mg_2Ni_{0.7}Ti_{0.3}$ alloys exhibited significantly reduced apparent dehydriding activation energies (E_a) of −46.12, −59.16 and −73.15 kJ/mol, respectively. A distinguishable reduction of dehydriding enthalpy was also observed for $Mg_2Ni_{0.7}Mn_{0.3}$ alloy. The anti-corrosion properties of $Mg_2Ni_{0.7}M_{0.3}$ alloy electrodes were also visibly improved compared with Mg_2Ni alloy.

2 Experimental

$Mg_2Ni_{0.7}M_{0.3}$ alloys were prepared by low-temperature solid phase sintering method. Firstly, the designed individual metal powder mixtures were homogeneously mixed on a planetary ball mill (QM−3SP2, China), and then pressed into pieces followed by being sintered at 853 K for 6 h in a tube furnace with the protection of high purity argon. The purities of starting materials (Mg, Ni, Al, Mn and Ti powders, from Sinopharm Chemical Reagent Co., Ltd.) were all higher than 99.99%.

The phase analysis was performed by powder X-ray diffraction (XRD) on a Philips X'Pert diffractometer (PANalytical X'Pert MRD) with Cu K_α radiation (λ= 1.54056 Å). Before starting the measurement, the zero shift of diffractometer system was calibrated by high purity silicon (with a purity of 99.999%). The lattice constants were calculated by Rietveld method using the X'Pert high score plus software. The microstructure and phase distribution were observed by scanning electron microscopy (SEM, ZEISS EVO18) and scanning transmission electron microscopy (STEM, FEI TALOS F200S).

The hydriding/dehydriding kinetics and pressure−composition isotherms (PCI) curves were measured by an automatic Sieverts apparatus (PCTPro E&E, SETARAM Inc., France). Before the experimental data collecting, 0.6000 g sample was fully activated by undergoing more than three cycles of hydrogen absorption/desorption at 573 K. The hydrogen absorption kinetics was measured under a starting pressure of 3 MPa. The hydrogen desorption kinetics was measured in nearly vacuum condition. The PCI measurements were carried out following the kinetics test. Finally, the Tafel curves were achieved using a standard test method on the instrument CHI660E (China).

3 Results and discussion

3.1 Phase analysis and microstructure

Figure 1 showed the XRD patterns of the as-sintered $Mg_2Ni_{0.7}M_{0.3}$ alloys. It was obviously observed that the FCC-structure intermetallic compounds of Mg_3AlNi_2, Mg_3MnNi_2 and Mg_3TiNi_2 (summarized as Mg_3MNi_2) formed in each alloy. It was considered that the intermetallic Mg_3MNi_2 compounds often coexisted with Mg when Mg_2Ni doped with mental elements, such as Al, Mn and Ti. Thus, element Mg was found in all alloys. For $Mg_2Ni_{0.7}Ti_{0.3}$ alloy, the amount of element Mg was even more than that of Mg_2Ni as judged by the intensity of the XRD peaks shown in Fig. 1(c). It could be found that the formation of intermetallic Mg_3TiNi_2 compound was difficult due to the large difference of atomic radius between Ti (2.00 Å) and Mg (1.72 Å), and the strong affinity of Ti and Ni led to the formation of Ni_3Ti. It was reported that the lattice sites of Mg (6i) in Mg_2Ni unit cell were replaced by three Mn atoms, resulting in the formation of cubic structure $Mg_9Mn_{3Mg(6i)}Ni_6$ compounds (normally written as Mg_3MnNi_2) [20,21]. Since Mg_3TiNi_2 was similar with Mg_3MnNi_2 in crystal structure, it could be naturally inferred that the difficulty of formation of Mg_3TiNi_2 was attributed to the large atomic radius of Ti. Based on Fig. 1, the lattice constants of Mg_3AlNi_2, Mg_3MnNi_2 and Mg_3TiNi_2 were calculated to be 1.1539(7), 1.1581(8) and 1.1617(6) nm, respectively. It was obvious that Mg_3TiNi_2 had the largest lattice constant. The stability of intermetallic Mg_3MNi_2 compounds could be related with the doped elements M. For example, ZHANG et al [21] reported that the stability of Mg_3AlNi_2 was the highest

among those intermetallic compounds. This was consistent with the present results, i.e. Mg_3TiNi_2 was more difficult to form than Mg_3MnNi_2 and Mg_3AlNi_2. So, it could be concluded that metal elements M with similar atomic radii to Mg were more beneficial to the formation and stability of intermetallic Mg_3MNi_2 compounds for the lower lattice distortion energy. Obviously, Mg_3TiNi_2 had the lowest stability among the intermetallic Mg_3MNi_2 compounds due to its high lattice distortion energy resulting from the largest Ti atomic radium. As a consequence, only small amount of Mg_3TiNi_2 was found in the $Mg_2Ni_{0.7}Ti_{0.3}$ alloy.

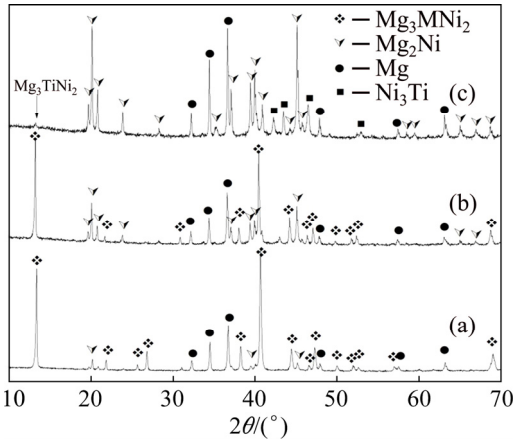

Fig. 1 Typical XRD patterns of sintered $Mg_2Ni_{0.7}M_{0.3}$ alloys: (a) $Mg_2Ni_{0.7}Al_{0.3}$; (b) $Mg_2Ni_{0.7}Mn_{0.3}$; (c) $Mg_2Ni_{0.7}Ti_{0.3}$

To explore the phase transition, the hydrogenated/dehydrogenated $Mg_2Ni_{0.7}Al_{0.3}$ alloys were subjected to powder XRD measurement, and the results were illustrated in Fig. 2. Figure 2(a) showed the XRD pattern of $Mg_2Ni_{0.7}Al_{0.3}$ alloy hydrogenated at 553 K, in which Mg_3AlNi_2, Mg_2NiH_4, $Mg_2NiH_{0.3}$ and MgO were identified. Because this sample was exposed to the open air for a long period, the elemental Mg was oxidized to MgO. Thus, MgH_2 was not found in the sample. This result also indicated that Mg_2Ni and Mg_3AlNi_2 were stable in the open air. The hydride of $Mg_3AlNi_2H_3$ was not found in the sample because of the over high hydriding temperature [18]. However, the solid solution of $Mg_2NiH_{0.3}$ was observed, which could form from dehydrogenation of Mg_2NiH_4 in cooling process. Figure 2(b) showed the XRD pattern of the dehydrogenated $Mg_2Ni_{0.7}Al_{0.3}$ alloy (not exposed to air). Obviously, the original phase components (Mg_2Ni, Mg_3AlNi_2 and Mg, Fig. 1(a)) were recovered from dehydrogenation, indicating a reversible phase transition upon hydriding and dehydriding for $Mg_2Ni_{0.7}Al_{0.3}$ alloy. That was to say, the hydrogenation of $Mg_2Ni_{0.7}Al_{0.3}$ alloy was fully reversible. The phase transition of $Mg_2Ni_{0.7}Mn_{0.3}$ and $Mg_2Ni_{0.7}Ti_{0.3}$ alloys was similar to that of $Mg_2Ni_{0.7}Al_{0.3}$ alloy.

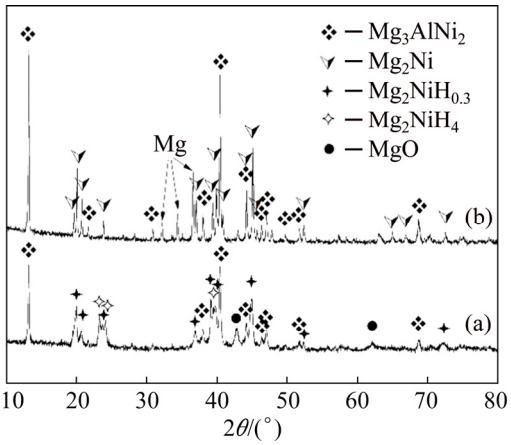

Fig. 2 Typical XRD patterns of $Mg_2Ni_{0.7}Al_{0.3}$ alloys: (a) As-hydrogenated at 553 K (stored in open air); (b) As-dehydrogenated (stored in glovebox)

Figure 3 showed the SEM and STEM images of $Mg_2Ni_{0.7}Al_{0.3}$ alloy. The backscattered electron image (Fig. 3(a)) illustrated that Mg_3AlNi_2 particles (marked with arrows) were embedded in the matrix of Mg and Mg_2Ni with a dimension of several micrometers. Mg and Mg_2Ni could not be distinguished by the back-

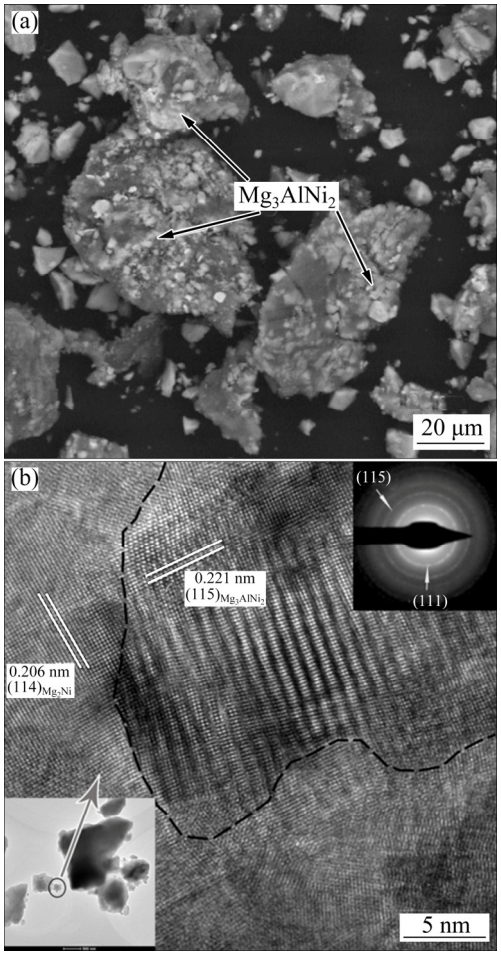

Fig. 3 SEM (a) and STEM (b) images of $Mg_2Ni_{0.7}Al_{0.3}$ alloy

scattered electron. For further investigating the microstructure, the electron diffraction was also performed and the results were illustrated in Fig. 3(b). The high-resolution lattice image combining the electron diffraction pattern indicated that Mg_3AlNi_2 was of a nanograin structure. Actually, the large particles of Mg_3AlNi_2, observed in Fig. 3(a), contained lots of nanograins. On the other hand, the grain boundaries between the Mg_3AlNi_2 and Mg_2Ni (or Mg) phases were not clear, showing a transitional layer with several atomic thicknesses. This special microstructure was possibly related to the formation mechanism of Mg_3AlNi_2. It was thought that three Al atoms substituted three Mg(6i) lattice sites in the Mg_2Ni unit cell, forming a cubic structure $Mg_9Al_{3Mg(6i)}Ni_6$ [20]. This formation mechanism could also explain why Mg_3AlNi_2 always coexisted with the elemental Mg in $Mg_2Ni_{0.7}Al_{0.3}$ alloy, as observed in Fig. 1(a).

3.2 Hydrogen storage properties

The rates of hydrogen absorption at different temperatures for $Mg_2Ni_{0.7}Al_{0.3}$, $Mg_2Ni_{0.7}Mn_{0.3}$ and $Mg_2Ni_{0.7}Ti_{0.3}$ alloys were measured and shown in Figs. 4(a)−(c), respectively. It could be observed that the $Mg_2Ni_{0.7}M_{0.3}$ alloys all had fairly good hydrogen absorption kinetics. The hydrogen absorption of $Mg_2Ni_{0.7}M_{0.3}$ alloys was all almost completed in 300 s at a low temperature of 493 K under a starting hydrogen pressure of 3 MPa. The hydriding kinetics of $Mg_2Ni_{0.7}M_{0.3}$ alloys was remarkably improved compared with pure Mg or Mg_2Ni [7,22], which could be related to the intermetallic compounds of Mg_3MNi_2. Although hydrides of $Mg_3MNi_2H_3$ were not found in the present experiments, it was reported that H atoms could dissolve in the octahedral and tetrahedral interstices in the lattice of Mg_3MnNi_2 [18]. However, the decomposition of H_2 molecules to H atoms was exactly a key barrier to block the quick hydrogen absorption of Mg-based alloys [23]. In fact, the PCI results indicated that Mg_3MNi_2 absorbed a small amount of hydrogen (about 0.3%, mass fraction). It was reasonably considered that H_2 molecules were firstly decomposed to H atoms and dissolved in the intermetallic Mg_3MNi_2 compounds, and then the H atoms transferred to Mg and Mg_2Ni, forming metal hydrides (MgH_2 and Mg_2NiH_4). Thus, the hydriding kinetics of Mg and Mg_2Ni was remarkably improved. Certainly, the nanograin structure and the phase boundaries also benefited to the improvement of hydrogen absorption, which was confirmed in many hydrogen storage material systems [16,22]. From Fig. 4, it could be also observed that the temperature did not significantly affect the hydrogen absorption rate when the hydriding temperature was higher than 493 K.

For practical utilization, it was confronted with a great challenge to improve the dehydriding kinetics. Accordingly, the dehydriding properties of $Mg_2Ni_{0.7}M_{0.3}$ alloys were systematically investigated. Figure 5 showed the dehydriding curves of $Mg_2Ni_{0.7}M_{0.3}$ alloys at different temperatures. It should be pointed out that $Mg_2Ni_{0.7}Al_{0.3}$ alloy did not complete hydrogen desorption at 493 and 513 K for dehydrogenation reaching equilibrium. The released hydrogen increased with the increase of dehydrding temperature due to the higher equilibrium pressure, and the hydrogen desorption rates were observably accelerated at the same time.

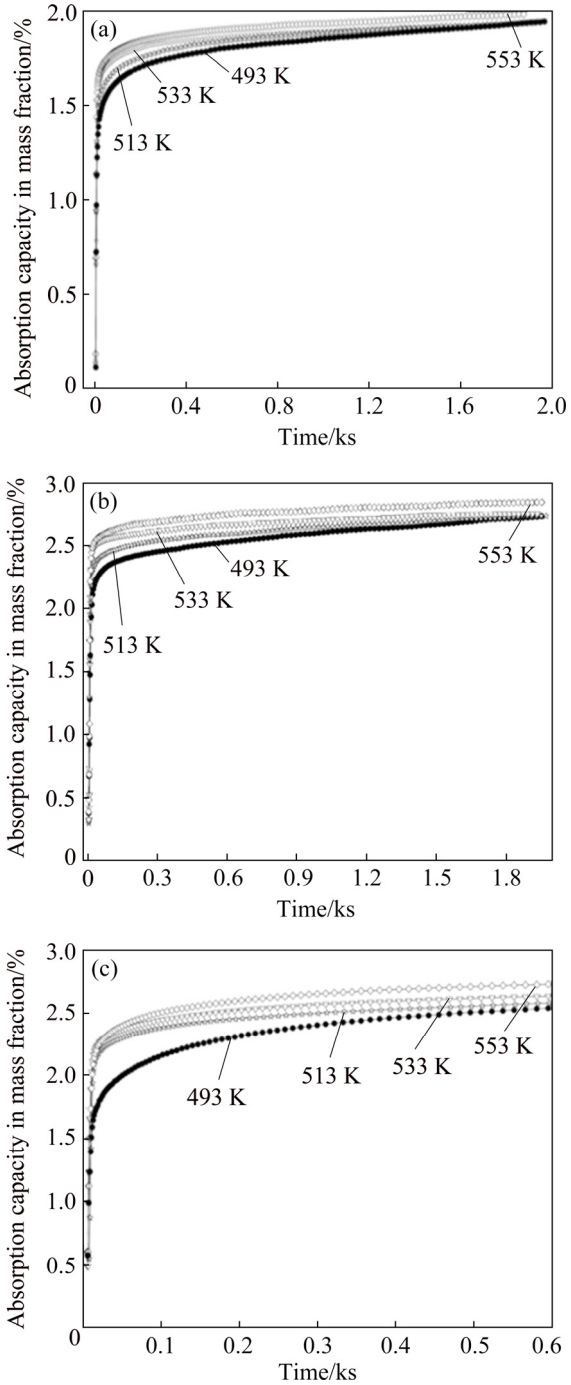

Fig. 4 Hydriding kinetics of $Mg_2Ni_{0.7}Al_{0.3}$ (a), $Mg_2Ni_{0.7}Mn_{0.3}$ (b) and $Mg_2Ni_{0.7}Ti_{0.3}$ (c)

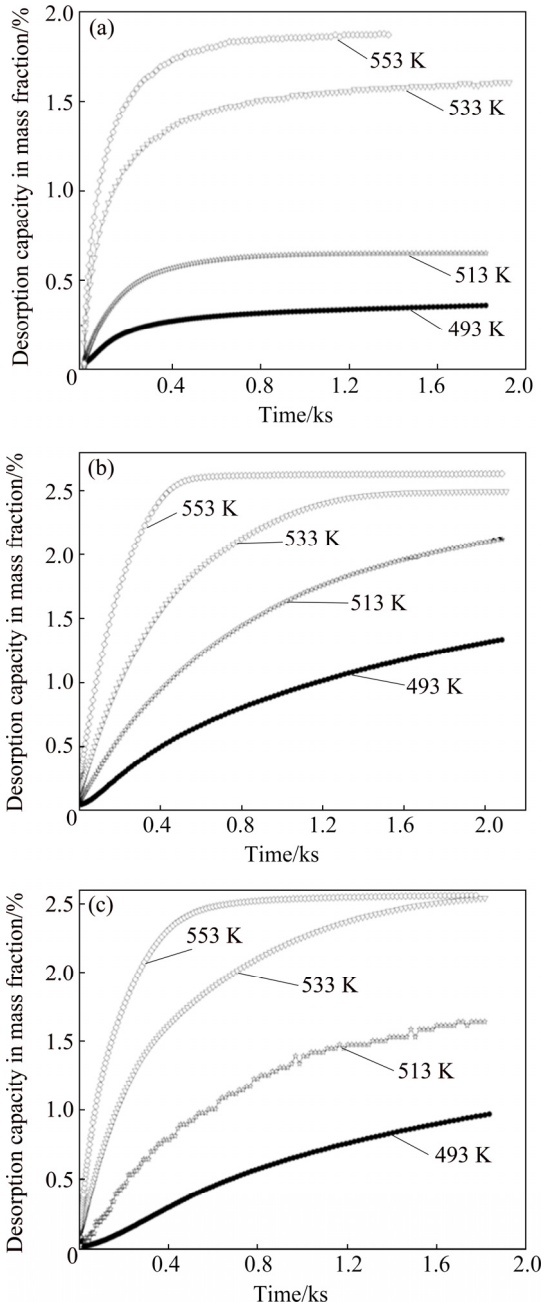

Fig. 5 Dehydriding curves of $Mg_2Ni_{0.7}Al_{0.3}$ (a), $Mg_2Ni_{0.7}Mn_{0.3}$ (b) and $Mg_2Ni_{0.7}Ti_{0.3}$ (c)

Figure 6 illustrated the Arrhenius plots for the dehydrogenation of $Mg_2Ni_{0.7}M_{0.3}$ alloys. The Arrhenius equation could be written as

$$K = K_0 \exp[-E_a/(RT)] \quad (1)$$

where K is the dehydriding reaction constant, which could be achieved by fitting the starting linear part of the hydrogen desorption curves (Fig. 5) using the Johnson−Mehl−Avrami−Kolmogorov (JMAK) equation; R is the mole gas constant; T is the hydrogen desorption temperature; E_a is the the apparent activation energy of dehydrogenation. By this method, E_a values were gotten to be −46.12, −59.16 and −73.15 kJ/mol for $Mg_2Ni_{0.7}Al_{0.3}$, $Mg_2Ni_{0.7}Mn_{0.3}$ and $Mg_2Ni_{0.7}Ti_{0.3}$ alloys, respectively, which were all far smaller than our previous reported values [24], and the recently reported values for Mg-based alloys [25].

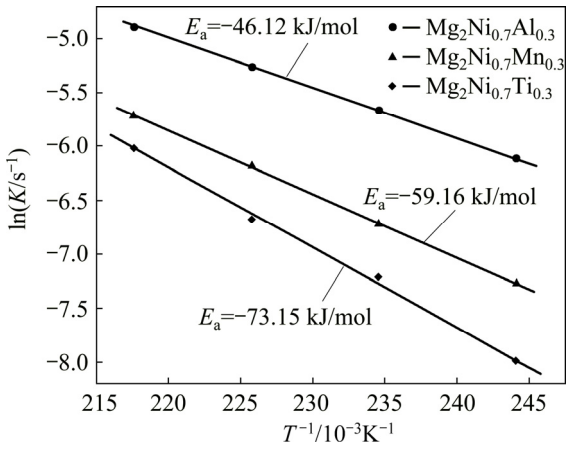

Fig. 6 Arrhenius plots for dehydrogenation of $Mg_2Ni_{0.7}M_{0.3}$ alloys

The high thermodynamic stability of hydrides was another critical challenge for Mg-based hydrogen storage materials. Thus, the thermodynamic destabilization of hydrides was a very crucial issue for hydrogen storage materials. Figure 7(a) showed the PCI curves of $Mg_2Ni_{0.7}Mn_{0.3}$ alloy at different temperatures. Observably, there were two plateaus respectively corresponding to the hydrogen absorption and desorption of Mg (marked as Plat. 1) and Mg_2Ni (marked as Plat. 2). The hydriding/dehydriding plateaus of Mg_3MnNi_2 did not exhibit in the PCI curves. This could be inferred that Mg_3MnNi_2 did not absorb hydrogen to transform to $Mg_3MnNi_2H_3$ at the studied temperatures because $Mg_3MnNi_2H_3$ was a room temperature stable hydride. This was consistent with the above XRD phase analysis. However, as observed in Figs. 7(a) and (b), $Mg_2Ni_{0.7}Al_{0.3}$ and $Mg_2Ni_{0.7}Mn_{0.3}$ alloys absorbed about 0.3% H_2 (mass fraction) when the pressure was higher than the Plat. 2. This capacity (0.3%) could be attributed to the dissolution of H atoms in the lattice interstice of $Mg_2Ni_{0.7}Mn_{0.3}$ and Mg_3MnNi_2, which could be confirmed by Fig. 7(b). Figure 7(b) illustrated the comparison of PCI curves for $Mg_2Ni_{0.7}Al_{0.3}$, $Mg_2Ni_{0.7}Mn_{0.3}$ and $Mg_2Ni_{0.7}Ti_{0.3}$ alloys at the same temperature of 533 K. The hydrogen capacity reduced with the increase of a mount of Mg_3MNi_2 in the alloys. For $Mg_2Ni_{0.7}Ti_{0.3}$ alloy, the capacity was the highest due to a trace of Mg_3TiNi_2 in the alloy. Unlike $Mg_2Ni_{0.7}Al_{0.3}$ and $Mg_2Ni_{0.7}Mn_{0.3}$ alloys, $Mg_2Ni_{0.7}Ti_{0.3}$ alloy had no obvious increase of capacity when the pressure was higher than Plat. 2. On the other hand, the hydriding/dehydriding plateau pressure of $Mg_2Ni_{0.7}M_{0.3}$

alloys increased a little due to the introduction of Mg_3MNi_2.

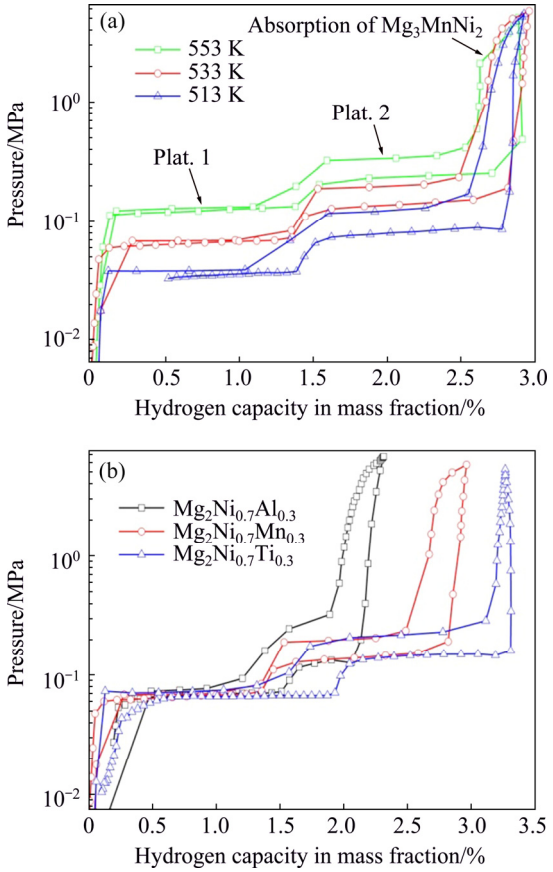

Fig. 7 PCI curves of $Mg_2Ni_{0.7}Mn_{0.3}$ alloys at different temperatures (a) and comparison of PCI curves of $Mg_2Ni_{0.7}M_{0.3}$ alloys at 533 K (b)

The hydriding/dehydriding thermodynamic properties were often evaluated by the hydriding/dehydriding enthalpy (ΔH) and entropy (ΔS), which could be calculated by vant' Hoff equation as follows:

$$\ln\left(\frac{p_{eq}}{p_0}\right)=\frac{\Delta H}{RT}-\frac{\Delta S}{R} \quad (2)$$

where p_{eq} and p_0 represent the equilibrium pressure and the standard atmospheric pressure, respectively. In this calculation, the equilibrium pressures (p_{eq}) were taken from the midpoint at the hydrogen desorption plateaus of Mg and Mg_2Ni in Fig. 7(a). The vant' Hoff plots for the dehydrogenation of $Mg_2Ni_{0.7}Mn_{0.3}$ alloy were illustrated in Fig. 8. The calculated enthalpies were (74.12±0.62) and (62.9±0.06) kJ/mol for Mg and Mg_2Ni, respectively, and the corresponding entropies were (135.45±1.91) and (120.91±0.12) J/(mol·K). The enthalpies had a distinguishable change compared with previous reported values for Mg (77.9 kJ/mol) [22] and Mg_2Ni (64.6 kJ/mol) [26]. The possible reasons for the reduction of dehydriding enthalpies could be attributed to the synergistic dehydriding effects among Mg, Mg_2Ni and Mg_3MnNi_2, as it was reported that $Mg_2NiH_{0.3}$ could enhance dehydriding of MgH_2 [27]. In fact, $Mg_2NiH_{0.3}$ could serve as a "hydrogen pump" for the dehydrogenation of MgH_2. As discussed above, the H atoms could also dissolve in the lattice of Mg_3MnNi_2. So, it could be inferred that Mg_3MnNi_2 could also have a similar effect with $Mg_2NiH_{0.3}$ on promoting hydrogen desorption of MgH_2 and Mg_2NiH_4. On the other hand, there were reports that the intermixed region and interfacial free energy could destabilize the hydrides [28]. Obviously, there were interfacial free energy and large amount of intermixed regions in $Mg_2Ni_{0.7}Mn_{0.3}$ alloy due to its nanograin microstructure. At last, the lattice elastic stress resulting from dehydrogenation could also have the destabilized effect on the adjacent hydrides [29]. Accordingly, a reduction of dehydriding enthalpies for MgH_2 and Mg_2NiH_4 was achieved upon $Mg_2Ni_{0.7}Mn_{0.3}$ alloy.

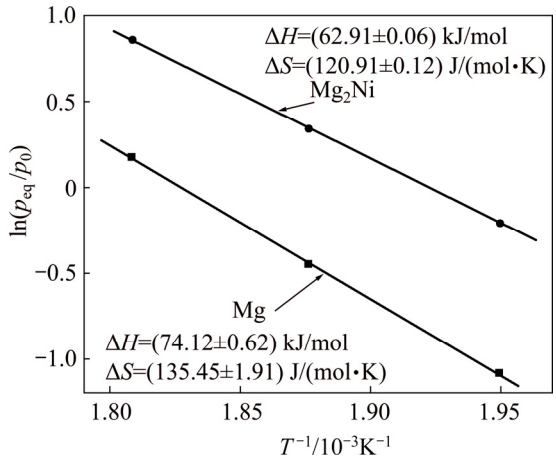

Fig. 8 Vant' Hoff plots for hydrogen desorption of Mg and Mg_2Ni

3.3 Corrosion resistance performance

As a promising electrode material of Ni−MH battery, it was also very important to improve the corrosion resistance of the Mg-based alloy in alkaline electrolyte [30,31]. Thus, the Tafel polarization curves of Mg_2Ni and $Mg_2Ni_{0.7}M_{0.3}$ alloy electrodes were measured and illustrated in Fig. 9. The electrochemical parameters related to corrosion (equilibrium potential φ_{corr}, linear polarization resistance R_p and corrosion current J_{corr}) were achieved by fitting the polarization cures (Fig. 9) and summarized in Table 1. Visibly, $Mg_2Ni_{0.7}M_{0.3}$ alloys had better corrosion resistance properties than Mg_2Ni alloy judging from J_{corr}. Compared with Mg_2Ni, the φ_{corr} of $Mg_2Ni_{0.7}M_{0.3}$ alloys shifted to the positive position, for example, there was a difference of 0.110 V between φ_{corr} values of $Mg_2Ni_{0.7}Al_{0.3}$ alloy (−0.529 V (vs SCE)) and Mg_2Ni (−0.639 V (vs SCE)), also indicating an improvement of corrosion resistance due to the addition of M elements. It was found that Mg_3MnNi_2 phase could

enhance the anti-corrosive performance of the particle surface of Mg_2Ni alloys [32]. In this work, the movement of φ_{corr} could be attributed to the introduction of Mg_3MNi_2 phases in the $Mg_2Ni_{0.7}M_{0.3}$ alloys. And there was another interesting phenomenon that the R_p of $Mg_2Ni_{0.7}Ti_{0.3}$ alloy was the highest among the $Mg_2Ni_{0.7}M_{0.3}$ alloy electrodes. It was reported that Mg_3MNi_2 could enhance the reaction activity and lower the pulverization rate of particles [32−34]. There was a trace of Mg_3TiNi_2 phase in the $Mg_2Ni_{0.7}Ti_{0.3}$ alloy, and it was thought that $Mg_2Ni_{0.7}Ti_{0.3}$ alloy had the maximum amount of Mg, thus leading to a thicker layer of $Mg(OH)_2$ covered on the electrode, which could block the movement of electrons. As a result, $Mg_2Ni_{0.7}Ti_{0.3}$ alloy showed a high R_p.

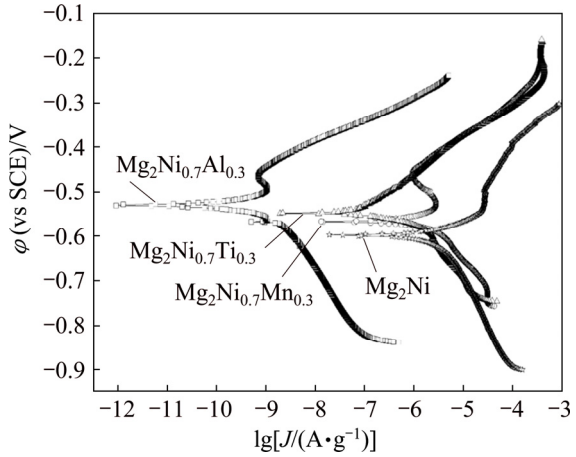

Fig. 9 Tafel polarization curves of Mg_2Ni and $Mg_2Ni_{0.7}M_{0.3}$ electrodes

Table 1 Electrochemical parameters related to corrosion

Sample	φ_{corr} (vs SCE)/V	$R_p/(\Omega\cdot g^{-1})$	$J_{corr}/(\mu A\cdot g^{-1})$
Mg_2Ni	−0.639	220	0.0472
$Mg_2Ni_{0.7}Ti_{0.3}$	−0.548	749	0.0242
$Mg_2Ni_{0.7}Al_{0.3}$	−0.529	354	0.0275
$Mg_2Ni_{0.7}Mn_{0.3}$	−0.579	287	0.0316

4 Conclusions

1) The FCC-structure intermetallic Mg_3MNi_2 compounds formed in $Mg_2Ni_{0.7}M_{0.3}$ (M = Al, Mn and Ti) alloys, and M element with atomic radius closer to Mg was more favorable to the formation of Mg_3MNi_2. H atoms could dissolve in the intermetallic Mg_3MNi_2 compounds forming solid solutions.

2) The intermetallic Mg_3MNi_2 compounds could accelerate the hydrogen adsorption and desorption of Mg-based alloys. The apparent activation energies of dehydrogenation reduced to be −46.12, −59.16 and −73.15 kJ/mol for $Mg_2Ni_{0.7}Al_{0.3}$, $Mg_2Ni_{0.7}Mn_{0.3}$ and $Mg_2Ni_{0.7}Ti_{0.3}$ alloys, respectively. And there was also a distinguishable reduction in dehydriding enthalpy for $Mg_2Ni_{0.7}M_{0.3}$ alloy.

3) Mg_3MNi_2 phase had positive effects on the improvement of anti-corrosion performances for $Mg_2Ni_{0.7}M_{0.3}$ alloys.

References

[1] CHEN Ping, ZHU Min. Recent progress in hydrogen storage [J]. Materials Today, 2008, 11: 36−43.

[2] ZHANG Yang-huan, HAN Zhong-gang, YUAN Ze-ming, YANG Tai, QI Yan, ZHAO Dong-liang. Electrochemical properties of nanocrystalline and amorphous Mg−Y−Ni alloys applied to Ni−MH battery [J]. Transactions of Nonferrous Metals Society of China, 2015, 25: 3736−3746.

[3] ZALUSKI L, ZALUSKA A, STRÖM-OLSEN J O. Hydrogen absorption in nanocrystalline Mg_2Ni formed by mechanical alloying [J]. Journal of Alloys and Compounds, 1995, 217: 245−249.

[4] SHAO Huai-yu, LI Xing-guo. Effect of nanostructure and partial substitution on gas absorption and electrochemical properties in Mg_2Ni-based alloys [J]. Journal of Alloys and Compounds, 2015, 667: 191−197.

[5] LI L Q, AKIYAMA T, YAGI J I. Activation behaviors of Mg_2NiH_4 at different hydrogen pressures in hydriding combustion synthesis [J]. International Journal of Hydrogen Energy, 2001, 26: 1035−1040.

[6] DARNAUDERY J P, DARRIET B, PEZAT M. The $Mg_2Ni_{0.75}M_{0.25}$ alloys (M = 3d element): Their application to hydrogen storage [J]. International Journal of Hydrogen Energy, 1983, 8: 705−708.

[7] GAO Jin-liang, SHANG Hong-wei, LI Ya-qin, YUAN Ze-ming, ZHAO Dong-liang, ZHANG Yang-huan. Gaseous storage hydrogen kinetics of La−Mg−Ni−Cu system Mg_2Ni type alloys [J]. The Chinese Journal of Nonferrous Metals, 2017, 27: 1132−1139. (in Chinese)

[8] ZHONG Hai-chang, WANG Hui. Microstructure and hydrogen storage properties of Mg(In) solid solutions [J]. The Chinese Journal of Nonferrous Metals, 2014, 24: 1486−1493. (in Chinese)

[9] XIE Li-shuai, LI Jin-shan, ZHANG Tie-bang, KOU Hong-chao. Role of milling time and Ni content on dehydrogenation behavior of MgH_2/Ni composite [J]. Transactions of Nonferrous Metals Society of China, 2017, 27: 569−577.

[10] ZHANG Yang-huan, LI Long-wei, FENG Dian-chen, GONG Peng-fei, SHANG Hong-wei, GUO Shi-hai. Hydrogen storage behavior of nanocrystalline and amorphous La−Mg−Ni-based $LaMg_{12}$-type alloys synthesized by mechanical milling [J]. Transactions of Nonferrous Metals Society of China, 2017, 27: 551−561.

[11] DING Xiao-li, LI Yong-tao, FANG Fang, SUN Da-lin, ZHANG Qing-an. Hydrogen-induced magnesium−zirconnim interfacial coupling: Enabling fast hydrogen sorption at lower temperatures [J]. Journal of Materials Chemistry A, 2017, 5: 5067−5076.

[12] ZHU Yun-feng, YANG Chen, ZHU Jin-yu, LI Li-quan. Structural and electrochemical hydrogen storage properties of Mg_2Ni-based alloys [J]. Journal of Alloys and Compounds, 2011, 509: 5309−5314.

[13] OHARA R, LAN C H, WANG C S. Electrochemical and structural characterization of nickel coating on Mg_2Ni hydrogen storage alloy [J]. Journal of Alloys and Compounds, 2013, 580(S): s368−s372.

[14] ZHAN L Y, ZHANG Y, ZHU Y F, ZHUANG X Y, WAN N, QU Y, GUO X L, CHEN J, WANG Z M, LI L Q. Electrochemical performances of $Mg_{45}M_5Co_{50}$ (M = Pd, Zr) ternary hydrogen storage electrodes [J]. Transactions of Nonferrous Metals Society of China, 2016, 26: 1388−1395.

[15] ZHONG H C, WANG H, LIU J W, SUN D L, ZHU M. Altered desorption enthalpy of MgH_2 by the reversible formation of Mg(In) solid solution [J]. Scripta Materialia, 2011, 65: 285−287.
[16] ZHONG H C, WANG H, OUYANG L Z. Improving the hydrogen storage properties of MgH_2 by reversibly forming Mg−Al solid solution alloys [J]. International Journal of Hydrogen Energy, 2014, 39: 3320−3326.
[17] WANG T M, ZHU Y F, ZHANG Y, LI L Q. Surface modification of Mg_3MnNi_2 hydrogen storage electrode alloy with polyaniline [J]. International Journal of Hydrogen Energy, 2017, 42: 14220−14226.
[18] DENYS R V, RIABOV A R, BEREZOVETS V V, KOVAL CHUK I V, ČERNÝ R, ZAVALIY I Y. Crystal structure of the novel $Mg_3MnNi_2D_{3-x}$ interstitial deuteride [J]. Intermetallics, 2011, 19: 1563−1566.
[19] ZHU M, GAO Y, CHE X Z, YANG Y Q, CHUNG C Y. Hydriding kinetics of nano-phase composite hydrogen storage alloys prepared by mechanical alloying of Mg and $M_mNi_{5-x}(CoAlMn)_x$ [J]. Journal of Alloys and Compounds, 2002, 330: 708−713.
[20] HUANG L W, ELKEDIM O, HAMZAOUI R. First principles investigation of the substitutional doping of Mn in Mg_2Ni phase and the electronic structure of Mg_3MnNi_2 phase [J]. Journal of Alloys and Compounds, 2011, 509: 328−333.
[21] ZHANG J, HUANG Y N, MAO C, PENG P, SHAO Y M, ZHOU D W. Ab initio calculations on energetics and electronic structures of cubic Mg_3MNi_2 (M = Al, Ti, Mn) hydrogen storage alloys [J]. International Journal of Hydrogen Energy, 2011, 36: 14477−14483.
[22] ZHONG H C, WANG H, OUYANG L Z, ZHU M. Microstructure and hydrogen storage properties of Mg−Sn nanocomposite by mechanical milling [J]. Journal of Alloys and Compounds, 2011, 509: 4268−4272.
[23] CUI J, WANG H, LIU J W, OUYANG L Z, ZHANG Q A, SUN D L, YAO X D, ZHU M. Remarkable enhancement in dehydrogenation of MgH_2 by a nano-coating of multi-valence Ti-based catalysts [J]. Journal of Materials Chemistry A, 2013, 1: 5603−5611.
[24] WANG H, ZHONG H C, OUYANG L Z, LIU J W, SUN D L, ZHANF Q A, ZHU M. Fully reversible de/hydriding of Mg base solid solutions with reduced reaction enthalpy and enhanced kinetics [J]. Journal of Physical Chemistry C, 2014, 118−123: 12087−12096.
[25] LAN Z Q, SUN Z Z, DING Y C, NING H, WEI W L, GUO J. Catalytic of Y_2O_3@graphene nanocomposites on the hydrogen-storage properties of Mg−Al alloys [J]. Journal of Materials Chemistry A, 2017, 5: 15200−15207.
[26] ZENG K J, KLASSEN T, OELERICH W, BORMANN R. Thermodynamic analysis of the hydriding process of Mg_2Ni alloys [J]. Journal of Alloys and Compounds, 1999, 283: 213−215.
[27] KALINICHENKA S, RONTZSCH L, KIEBACK B. Structural and hydrogen storage properties of melt-spun Mg−Ni−Y alloys [J]. International Journal of Hydrogen Energy, 2009, 34: 7749−7755.
[28] OUYANG L Z, YE S Y, DONG H W, ZHU M. Effect of interfacial free energy on hydriding reaction of Mg−Ni thin films [J]. Applied Physics Letter, 2007, 90(2): 21917−21919.
[29] BALDI A, GONZALEZ-SILVEIRA M, PALMISANO V, DAM B, GRIESSEN R. Destabilization of the Mg−H system through elastic constraints [J]. Physical Review Letter, 2009, 102: 226102−226106.
[30] NIU H, NORTHWOOD D O. Enhanced electrochemical properties of ball-milled Mg_2Ni electrodes [J]. International Journal of Hydrogen Energy, 2002, 27: 69−77.
[31] DU Q, LI S, HUANG G, FENG Q. Enhanced electrochemical kinetics of magnesium-based hydrogen storage alloy by mechanical milling with graphite [J]. International Journal of Hydrogen Energy, 2017, 42: 21871−21879.
[32] HSU F K, LIN C K, LEE S L, LIN C Y, BOR H Y. Effect of Mg_3MnNi_2 on the electrochemical characteristics of Mg_2Ni electrode alloy [J]. Journal of Power Sources, 2010, 195: 374−379.
[33] HUANG L W, ELKEDIM O, JARZEBSKI M, HAMZAOUI R, JURCZYK M. Structural characterization and electrochemical hydrogen storage properties of $Mg_2Ni_{1-x}Mn_x$ (x = 0, 0.125, 0.250, 0.375) alloys prepared by mechanical alloying [J]. International Journal of Hydrogen Energy, 2010, 35: 6794−6803.
[34] YANG Xiao-wei, ZHU Yun-feng, ZHANG Ji-guang, ZHANG Yao, LIU Ya-na, LIN Huai-jun, WANG Tai-miao, LI Li-quan. Effect of partial substitution of Ti for Al on the phase structure and electrochemical hydrogen storage properties of Mg_3AlNi_2 alloy [J]. Journal of Alloys and Compounds, 2018, 746: 421−427.

添加金属元素 Al、Mn 和 Ti 后 Mg_2Ni 合金的显微组织及其显著改善的储氢性能

钟海长[1,2]，徐敬博[2]，姜春海[1,2]，卢向军[1,2]

1. 厦门理工学院 功能材料及其应用福建省重点实验室，厦门 361024；
2. 厦门理工学院 材料科学与工程学院，厦门 361024

摘 要：采用固相烧结方法制备 $Mg_2Ni_{0.7}M_{0.3}$ (M = Al, Mn, Ti)合金。利用 X 射线衍射仪、扫描电镜和扫描透射电镜对合金的相组成和显微组织进行系统表征。结果发现，$Mg_2Ni_{0.7}M_{0.3}$ 合金中形成了具有面心立方结构的金属间化合物 Mg_3MNi_2，其与 Mg 和 Mg_2Ni 共存；且 M 原子半径与 Mg 原子半径越接近，越有利于 Mg_3MNi_2 的形成。采用 Sievert 和 Tafel 方法对 $Mg_2Ni_{0.7}M_{0.3}$ 合金的储氢性能和耐腐蚀性能进行研究。$Mg_2Ni_{0.7}M_{0.3}$ 合金的吸/放氢性能得到明显改善。$Mg_2Ni_{0.7}Al_{0.3}$、$Mg_2Ni_{0.7}Mn_{0.3}$ 和 $Mg_2Ni_{0.7}Ti_{0.3}$ 合金的脱氢反应的激活能较 Mg_2Ni 的激活能明显降低，分别为−46.12、−59.16 和−73.15 kJ/mol。与 Mg_2Ni 合金相比，$Mg_2Ni_{0.7}M_{0.3}$ 合金的腐蚀电位向正方向移动，如 $Mg_2Ni_{0.7}Al_{0.3}$ 合金(−0.529 V)与 Mg_2Ni 合金(−0.639 V)的腐蚀电位差为 0.110 V，表明添加 Al、Mn 和 Ti 能使合金的耐腐蚀性能得到显著提高。

关键词：Mg_2Ni；Mg_3MNi_2；吸氢动力学；脱氢激活能；耐腐蚀性能

(Edited by Wei-ping CHEN)